

Inclusive charged-current neutrino-nucleus reactions calculated with the relativistic quasiparticle random phase approximation

N. Paar, D. Vretenar, and T. Marketin

Physics Department, Faculty of Science, University of Zagreb, Croatia

P. Ring

Physik-Department der Technischen Universität München, D-85748 Garching, Germany

(Dated: March 5, 2022)

Abstract

Inclusive neutrino-nucleus cross sections are calculated using a consistent relativistic mean-field theoretical framework. The weak lepton-hadron interaction is expressed in the standard current-current form, the nuclear ground state is described with the relativistic Hartree-Bogoliubov model, and the relevant transitions to excited nuclear states are calculated in the relativistic quasiparticle random phase approximation. Illustrative test calculations are performed for charged-current neutrino reactions on ^{12}C , ^{16}O , ^{56}Fe , and ^{208}Pb , and results compared with previous studies and available data. Using the experimental neutrino fluxes, the averaged cross sections are evaluated for nuclei of interest for neutrino detectors. We analyze the total neutrino-nucleus cross sections, and the evolution of the contribution of the different multipole excitations as a function of neutrino energy. The cross sections for reactions of supernova neutrinos on ^{16}O and ^{208}Pb target nuclei are analyzed as functions of the temperature and chemical potential.

PACS numbers: 21.30.Fe, 21.60.Jz, 23.40.Bw, 25.30.-c

I. INTRODUCTION

Neutrino-nucleus reactions at low energies play an important role in many phenomena in nuclear and particle physics, as well as astrophysics. These reactions present extremely subtle physical processes, not only because they involve the weak interaction, but also because they are very sensitive to the structure of nuclear ground states and excitations, i.e. to the solution of the nuclear many-body problem that includes the strong and electromagnetic interactions. The use of microscopic nuclear structure models in a consistent theoretical framework is therefore essential for a quantitative description of neutrino-nucleus reactions [1]. Detailed predictions of neutrino-nucleus cross sections are crucial for the interpretation of neutrino experiments, detection of neutrinos produced in supernova explosions and understanding the underlying nature of these explosions [2]. Neutrino-nucleus reactions which occur in a type II supernova could also contribute to the nucleosynthesis [3, 4], but more data on cross sections are necessary for a more complete understanding of this process, as well as the supernova dynamics.

Data on neutrino-nucleus cross sections have been obtained by the LSND [5, 6] and KARMEN [7, 8, 9] collaborations, and at LAMPF [10, 11], but only for ^{12}C and ^{56}Fe target nuclei. New experimental programs are being planned which will provide essential data on the neutrino-nucleus reactions, and also help to improve the reliability of present cross-section calculations. These include the spallation neutron source (SNS) at ORNL, where neutrinos produced by pion decay at rest will enable measurements of cross sections for a wide range of target nuclei [12, 13], and the promising “beta-beams” method for the production of pure electron neutrino-beams by using the β -decay of boosted radioactive ions [14, 15]. Cross sections for neutrino energies in the range of tens of MeV could be measured, and these reactions are particularly interesting for supernova studies [16].

Weak interaction rates at low energies have been analyzed employing a variety of microscopic approaches, principally in the frameworks of the shell model [17, 18, 19], the random phase approximation (RPA) [20, 21, 22, 23], continuum RPA (CRPA) [24, 25, 26, 27, 28], hybrid models of CRPA and shell model [29, 30], and the Fermi gas model [31, 32, 33]. The shell model provides a very accurate description of ground state wave functions. The description of high-lying excitations, however, necessitates the use of large model spaces and this often leads to computational difficulties, making the approach applicable essentially only to

light and medium-mass nuclei. For systematic studies of weak interaction rates throughout the nuclide chart, microscopic calculations must therefore be performed using models based on the RPA.

Hybrid models combine the shell-model and CRPA in such a way that occupation probabilities of single-particle states in a specific nucleus are determined by shell model calculations, and then inserted into the CRPA [29]. In general the CRPA employs different interactions for the calculation of the nuclear ground state (for instance, the Woods-Saxon potential), and in the residual CRPA interaction (G matrix from the Bonn potential, or the Landau-Migdal interaction), and thus additional parameters are required in order to adjust the calculated rates to data. A more consistent approach, based on the quasiparticle RPA with Skyrme effective interactions, has been employed in calculations of weak interaction rates [22]. Although in this framework the residual RPA interaction is derived from the same energy functional which determines the nuclear ground state, some terms are usually omitted, and pairing correlations require the adjustment of additional factors. A fully consistent theoretical framework for the description of charge-exchange excitations in open shell nuclei, based on Skyrme effective interactions, has only recently been developed [34], but not yet employed in the analysis of neutrino-nucleus reactions. Neutrino-nucleus cross sections have also been calculated using the ab-initio no-core shell model based on realistic NN and three-body interactions [35], and the shell model with an improved Hamiltonian which properly takes into account the spin-isospin interactions [36]. The importance of improved calculations of neutrino-nucleus cross sections for neutrino-oscillation studies has been demonstrated in the recent reanalysis of the LSND experiment [37], using the particle-number projected quasiparticle RPA [38], which has shown an enhancement of the neutrino-oscillation probability when compared to previous studies.

Although the general expressions for the transition matrix elements relevant for the calculation of neutrino-nucleus cross sections have been known since many years [39, 40], it is only more recently that systematic calculations have been performed in open-shell nuclei by making use of modern effective interactions in the description of both nuclear ground states and excitations [22]. Reliable prediction of weak interaction rates in nuclei necessitates a fully consistent description of the structure of ground states and multipole excitations. Among the relevant charge-exchange excitations, the isobaric analog state (IAS) and Gamow-Teller resonance (GTR) have been the subject of extensive experimental and theoretical studies.

Much more limited are the data and theoretical predictions for properties of excitations of higher multiplicities at finite momentum transfer.

In this work we analyze charged-current neutrino-nucleus reactions by employing a fully consistent microscopic approach based on relativistic energy density functionals, and also including pairing correlations in the description of open-shell target nuclei. An essential advantage over most current approaches is the use of a single universal effective interaction in calculations of both ground-state properties and multipole excitations of nuclei in various mass regions of the chart of nuclides.

Of particular interest for the present study are rates for neutrino-nucleus reactions in the low-energy range below 100 MeV, which play an important role in many astrophysical processes, including stellar nucleosynthesis. A quantitative description of nucleosynthesis of heavy elements during the r-process necessitates accurate predictions of neutrino-nucleus cross sections not only in stable nuclei, but also in nuclei away from the valley of β -stability. Since nuclei are used as detectors for solar and supernovae neutrinos, as well as in neutrino oscillation experiments, it is important to describe the neutrino detector response in a consistent and fully microscopic theory. Finally, a quantitative estimate of neutrino-nucleus reaction rates will provide information relevant for feasibility studies and simulations of a low-energy beta beam facility, which could be used to produce neutrino beams of interest for particle physics, nuclear physics and astrophysics [15].

In Sec. II we outline the basic formalism used in the evaluation of neutrino-nucleus cross sections. In Sec. III the relativistic Hartree-Bogoliubov model (RHB), and the proton-neutron relativistic quasiparticle random phase approximation (PN-RQRPA) are briefly reviewed. Section IV includes several test cases, and the calculated cross sections are compared with results of previous theoretical studies and the available data. Cross sections for supernova neutrinos are analyzed in Sec. V, and finally Sec. VI summarizes the results of the present investigation and ends with an outlook for future studies.

II. NEUTRINO-NUCLEUS CROSS SECTIONS

In the present study we consider the charged-current neutrino-nucleus reactions:

$$\nu_l + {}_Z X_N \rightarrow {}_{Z+1} X_{N-1}^* + l^- , \quad (1)$$

where l denotes the charged lepton (electron, muon). Detailed expressions for the reaction rates and the transition matrix elements can be found in Refs. [31, 39]. The charged-current neutrino-nucleus cross section reads

$$\left(\frac{d\sigma_\nu}{d\Omega}\right) = \frac{1}{(2\pi)^2} V^2 p_l E_l \sum_{\substack{\text{lepton} \\ \text{spins}}} \frac{1}{2J_i + 1} \sum_{M_i M_f} |\langle f | \hat{H}_W | i \rangle|^2, \quad (2)$$

where p_l and E_l are the momentum and energy of the outgoing lepton, respectively. The Hamiltonian \hat{H}_W of the weak interaction is expressed in the standard current-current form, i.e. in terms of the nucleon $\mathcal{J}_\lambda(\mathbf{x})$ and lepton $j_\lambda(\mathbf{x})$ currents

$$\hat{H}_W = -\frac{G}{\sqrt{2}} \int d\mathbf{x} \mathcal{J}_\lambda(\mathbf{x}) j^\lambda(\mathbf{x}), \quad (3)$$

and the transition matrix elements read

$$\langle f | \hat{H}_W | i \rangle = -\frac{G}{\sqrt{2}} l_\lambda \int d\mathbf{x} e^{-i\mathbf{q}\mathbf{x}} \langle f | \mathcal{J}^\lambda(\mathbf{x}) | i \rangle. \quad (4)$$

The multipole expansion of the leptonic matrix element $l_\lambda e^{-i\mathbf{q}\mathbf{x}}$ determines the operator structure for the nuclear transition matrix elements [31], and the expression for the neutrino-nucleus cross section. In the *extreme relativistic limit*— (ERL), in which the energy of the outgoing lepton is considered much larger than its rest mass, the differential neutrino-nucleus cross section takes the form

$$\begin{aligned} \left(\frac{d\sigma_\nu}{d\Omega}\right)_{ERL} &= \frac{2G_F^2 \cos^2 \theta_c}{\pi} \frac{E_l^2}{2J_i + 1} \\ &\times \left\{ \left(\frac{q^2}{2\mathbf{q}^2} \cos^2 \frac{\theta}{2} + \sin^2 \frac{\theta}{2} \right) \sum_{J \geq 1} \left[|\langle J_f | \hat{\mathcal{T}}_J^{MAG} | J_i \rangle|^2 + |\langle J_f | \hat{\mathcal{T}}_J^{EL} | J_i \rangle|^2 \right] \right. \\ &- \sin \frac{\theta}{2} \sqrt{\frac{q^2}{\mathbf{q}^2} \cos^2 \frac{\theta}{2} + \sin^2 \frac{\theta}{2}} \sum_{J \geq 0} 2 \text{Re} \langle J_f | \hat{\mathcal{T}}_J^{MAG} | J_i \rangle \langle J_f | \hat{\mathcal{T}}_J^{EL} | J_i \rangle^* \\ &\left. + \cos^2 \frac{\theta}{2} \sum_{J \geq 0} \left| \langle J_f | \hat{\mathcal{M}}_J - \frac{q_0}{|\mathbf{q}|} \hat{\mathcal{L}}_J | J_i \rangle \right|^2 \right\}. \quad (5) \end{aligned}$$

where G_F is the Fermi constant for the weak interaction, θ_c is the Cabbibo's angle, θ denotes the angle between the incoming and outgoing leptons, the energy of the lepton in the final state is E_l , and the 4-momentum transfer is $q \equiv (q_0, \mathbf{q})$. The nuclear transition matrix elements between the initial state $|J_i\rangle$ and final state $|J_f\rangle$, correspond to the charge $\hat{\mathcal{M}}_J$, longitudinal $\hat{\mathcal{L}}_J$, transverse electric $\hat{\mathcal{T}}_J^{EL}$, and transverse magnetic $\hat{\mathcal{T}}_J^{MAG}$ multipole

operators. These are expressed in terms of spherical Bessel functions, spherical harmonics, and vector spherical harmonics:

$$M_J^M \equiv j_J(\kappa x) Y_J^M(\Omega_x) \quad (6)$$

$$\mathbf{M}_{JL}^M \equiv j_L(\kappa x) \mathbf{Y}_{JL1}^M(\Omega_x), \quad (7)$$

where we use the standard notation $\kappa = |\mathbf{q}|$. There are four transition operators in Eq. (5):

- the Coulomb multipole operator

$$\hat{\mathcal{M}}_{JM}(\mathbf{x}) = F_1^V M_J^M(\mathbf{x}) - i \frac{\kappa}{m_N} \left[F_A \Omega_J^M(\mathbf{x}) + \frac{1}{2} (F_A - q_0 F_P) \Sigma_J^{\prime\prime M}(\mathbf{x}) \right], \quad (8)$$

- the longitudinal operator

$$\hat{\mathcal{L}}_{JM}(\mathbf{x}) = -\frac{q_0}{\kappa} F_1^V M_J^M(\mathbf{x}) + i \left[F_A - \frac{1}{2} \frac{\kappa^2}{m_N} F_P \right] \Sigma_J^{\prime\prime M}(\mathbf{x}), \quad (9)$$

- the transverse electric operator

$$\hat{\mathcal{T}}_{JM}^{el}(\mathbf{x}) = \frac{\kappa}{m_N} \left[F_1^V \Delta_J^M(\mathbf{x}) + \frac{1}{2} \mu^V \Sigma_J^M(\mathbf{x}) \right] + i F_A \Sigma_J^{\prime M}(\mathbf{x}), \quad (10)$$

- and the transverse magnetic operator

$$\hat{\mathcal{T}}_{JM}^{mag}(\mathbf{x}) = -i \frac{\kappa}{m_N} \left[F_1^V \Delta_J^M(\mathbf{x}) - \frac{1}{2} \mu^V \Sigma_J^{\prime M}(\mathbf{x}) \right] + F_A \Sigma_J^M(\mathbf{x}), \quad (11)$$

where all the form factors are functions of q^2 . These multipole operators contain seven fundamental operators expressed in terms of spherical Bessel functions, spherical harmonics, and vector spherical harmonics [39]:

$$M_J^M(\mathbf{x}) \quad (12)$$

$$\Delta_J^M(\mathbf{x}) = \mathbf{M}_{JJ}^M(\mathbf{x}) \frac{1}{\kappa} \nabla \quad (13)$$

$$\Delta_J^{\prime M}(\mathbf{x}) = \left[-\sqrt{\frac{J}{2J+1}} \mathbf{M}_{JJ+1}^M(\mathbf{x}) + \sqrt{\frac{J+1}{2J+1}} \mathbf{M}_{JJ-1}^M(\mathbf{x}) \right] \frac{1}{\kappa} \nabla \quad (14)$$

$$\Sigma_J^M(\mathbf{x}) = \mathbf{M}_{JJ}^M(\mathbf{x}) \boldsymbol{\sigma} \quad (15)$$

$$\Sigma_J^{\prime M}(\mathbf{x}) = \left[-\sqrt{\frac{J}{2J+1}} \mathbf{M}_{JJ+1}^M(\mathbf{x}) + \sqrt{\frac{J+1}{2J+1}} \mathbf{M}_{JJ-1}^M(\mathbf{x}) \right] \boldsymbol{\sigma} \quad (16)$$

$$\Sigma_J^{\prime\prime M}(\mathbf{x}) = \left[\sqrt{\frac{J+1}{2J+1}} \mathbf{M}_{JJ+1}^M(\mathbf{x}) + \sqrt{\frac{J}{2J+1}} \mathbf{M}_{JJ-1}^M(\mathbf{x}) \right] \boldsymbol{\sigma} \quad (17)$$

$$\Omega_J^M(\mathbf{x}) = M_J^M(\mathbf{x})\boldsymbol{\sigma}\frac{1}{\kappa}\boldsymbol{\nabla}. \quad (18)$$

By assuming conserved vector current (CVC), the standard set of form factors reads [33, 39]:

$$F_1^V(q^2) = \left(1 + \frac{q^2}{(855\text{MeV})^2}\right)^{-2} \quad (19)$$

$$\mu^V(q^2) = 4.706 \left(1 + \frac{q^2}{(855\text{MeV})^2}\right)^{-2} \quad (20)$$

$$F_A(q^2) = -1.23 \left(1 + \frac{q^2}{(855\text{MeV})^2}\right)^{-2} \quad (21)$$

$$F_P(q^2) = \frac{2m_N F_A(q^2)}{q^2 + m_\pi^2}. \quad (22)$$

The neutrino-nucleus cross section is evaluated using Eq. (5), with the transition matrix elements between the initial and final states determined in a fully microscopic theoretical framework based on the Relativistic Hartree-Bogoliubov (RHB) model for the nuclear ground state, and excited states are calculated using the relativistic quasiparticle random phase approximation (RQRPA). More details about the RHB+RQRPA framework are presented in the next section.

III. THE PROTON-NEUTRON RELATIVISTIC QUASIPARTICLE RANDOM PHASE APPROXIMATION

Here we outline the essential features of the theoretical framework that will be used to evaluate inclusive neutrino-nucleus cross sections: the proton-neutron (PN)-RQRPA based on relativistic Hartree-Bogoliubov model. The detailed formalism, as well as recent applications of these models in the description of exotic structure phenomena in nuclei far from stability, have been reviewed in Refs. [41, 42].

The RQRPA has been formulated in the canonical single-nucleon basis of the relativistic Hartree-Bogoliubov (RHB) model in Ref. [43], and extended to the description of charge-exchange excitations (proton-neutron RQRPA) in Ref. [44]. In the RHB framework the ground state of a nucleus can be written either in the quasiparticle basis as a product of independent quasi-particle states, or in the canonical basis as a highly correlated BCS-state. By definition, the canonical basis diagonalizes the density matrix and is always localized. It describes both the bound states and the positive-energy single-particle continuum. The

QRPA equations in the canonical basis include the matrix elements $V_{\kappa\lambda'\kappa'\lambda}^{ph}$ of the residual particle-hole (ph) interaction, and the matrix elements $V_{\kappa\kappa'\lambda\lambda'}^{pp}$ of the particle-particle (pp) (pairing) interaction, as well as certain combinations of occupation factors u_κ , v_κ of the canonical single-nucleon states. In addition to the configurations built from two-quasiparticle states of positive energy, the relativistic QRPA configuration space must also include pair-configurations formed from the fully or partially occupied states of positive energy and the empty negative-energy states from the Dirac sea. The inclusion of configurations built from occupied positive-energy states and empty negative-energy states is essential for current conservation, decoupling of spurious states, and a quantitative description of excitation energies of giant resonances [43].

The RHB+RQRPA model is fully consistent: in the particle-hole channel effective Lagrangians with density-dependent meson-nucleon couplings are employed, and pairing correlations are described by the pairing part of the finite range Gogny interaction [45]. Both in the ph and pp channels, the same interactions are used in the RHB equations that determine the canonical quasiparticle basis, and in the matrix equations of the RQRPA. This is very important because the energy weighted sum rules are fulfilled only if the pairing interaction is consistently included both in the static RHB and in the dynamical RQRPA calculation. In the present work all RHB plus QRPA calculations have been performed using one of the modern and most accurate meson-exchange density-dependent relativistic mean-field effective interactions – DD-ME2 [50] in the ph channel, and the finite range Gogny interaction D1S [45] in the pp channel.

Charge-exchange excitations have been analyzed with the proton-neutron RQRPA using effective Lagrangians characterized by density-dependent meson-nucleon couplings [44]. The RHB plus PN-RQRPA framework has been successfully employed in studies of isobaric analog resonances, Gamow-Teller resonances [44], the relation between the excitation energies of IAS and GTR and the evolution of neutron skin in neutron-rich nuclei [46], and β -decay rates of r-process nuclei [47, 48]. The model includes both the $T = 1$ and $T = 0$ pairing channels, and represents a relativistic extension of the fully-consistent proton-neutron QRPA introduced in Ref. [49].

The matrix equations of the PN-RQRPA read

$$\begin{pmatrix} A & B \\ B^* & A^* \end{pmatrix} \begin{pmatrix} X^\lambda \\ Y^\lambda \end{pmatrix} = E_\lambda \begin{pmatrix} 1 & 0 \\ 0 & -1 \end{pmatrix} \begin{pmatrix} X^\lambda \\ Y^\lambda \end{pmatrix}, \quad (23)$$

with the matrices A and B defined in the canonical basis

$$\begin{aligned} A_{pn,p'n'} &= H_{pp'}^{11} \delta_{nn'} + H_{nn'}^{11} \delta_{pp'} \\ &\quad + (u_p v_n u_{p'} v_{n'} + v_p u_n v_{p'} u_{n'}) V_{pn'np'}^{ph} + (u_p u_n u_{p'} u_{n'} + v_p v_n v_{p'} v_{n'}) V_{pnp'n'}^{pp} \\ B_{pn,p'n'} &= (u_p v_n v_{p'} u_{n'} + v_p u_n u_{p'} v_{n'}) V_{pp'nn'}^{ph} \\ &\quad - (u_p u_n v_{p'} v_{n'} + v_p v_n u_{p'} u_{n'}) V_{pnp'n'}^{pp}. \end{aligned} \quad (24)$$

The proton and neutron quasiparticle canonical states are denoted by p , p' , and n , n' , respectively. V^{ph} is the proton-neutron particle-hole residual interaction, and V^{pp} denotes the particle-particle interaction. The canonical basis diagonalizes the density matrix, and the corresponding eigenvalues are the occupation probabilities $v_{p(n)}^2$. Since on the other hand the canonical basis does not diagonalize the Dirac single-nucleon mean-field Hamiltonian \hat{h}_D , nor the pairing field $\hat{\Delta}$, the off-diagonal matrix elements $H_{nn'}^{11}$, and $H_{pp'}^{11}$, appear in Eq. (24):

$$H_{\kappa\kappa'}^{11} = (u_\kappa u_{\kappa'} - v_\kappa v_{\kappa'}) h_{\kappa\kappa'} - (u_\kappa v_{\kappa'} + v_\kappa u_{\kappa'}) \Delta_{\kappa\kappa'}. \quad (25)$$

The solution of the RQRPA matrix equation (23) determines the excitation energies E_λ and the corresponding forward- and backward-going amplitudes X^λ and Y^λ , respectively. In the evaluation of the neutrino-nucleus cross section (Eq. (5)), for each transition operator \hat{O}^J the matrix elements between the ground state of the even-even (N,Z) target nucleus and the final state are expressed in terms of single-particle matrix elements between quasiparticle canonical states, occupation probabilities, and the corresponding RQRPA amplitudes:

$$\langle J_f || \hat{O}^J || J_i \rangle = \sum_{pn} \langle p || \hat{O}^J || n \rangle (X_{pn}^J u_p v_n - Y_{pn}^J v_p u_n). \quad (26)$$

In the calculations performed in this work we have considered transitions between the $|0^+\rangle$ ground state of a spherical even-even target nucleus and excited states in the odd-odd nucleus with multiplicities $J_f^\pi = 0^\pm - 7^\pm$.

The spin-isospin-dependent interaction terms are generated by the exchange of π and ρ mesons. Although the direct one-pion contribution to the nuclear ground state vanishes at the mean-field level because of parity conservation, the pion nevertheless must be included

in the calculation of spin-isospin excitations which contribute to the neutrino-nucleus cross section. The corresponding particle-hole residual interaction of the PN-RQRPA is derived from the Lagrangian density

$$\mathcal{L}_{\pi+\rho}^{int} = -g_\rho \bar{\psi} \gamma^\mu \vec{\rho}_\mu \vec{\tau} \psi - \frac{f_\pi}{m_\pi} \bar{\psi} \gamma_5 \gamma^\mu \partial_\mu \vec{\pi} \vec{\tau} \psi, \quad (27)$$

where arrows denote vectors in isospin space. The residual two-body interaction reads

$$\begin{aligned} V(\mathbf{r}_1, \mathbf{r}_2) &= \vec{\tau}_1 \vec{\tau}_2 (\beta \gamma^\mu)_1 (\beta \gamma_\mu)_2 g_\rho [\rho_v(\mathbf{r}_1)] g_\rho [\rho_v(\mathbf{r}_2)] D_\rho(\mathbf{r}_1, \mathbf{r}_2) \\ &- \left(\frac{f_\pi}{m_\pi} \right)^2 \vec{\tau}_1 \vec{\tau}_2 (\Sigma_1 \nabla_1) (\Sigma_2 \nabla_2) D_\pi(\mathbf{r}_1, \mathbf{r}_2), \end{aligned} \quad (28)$$

where $D_{\rho(\pi)}$ is the meson propagator

$$D_{\rho(\pi)} = \frac{1}{4\pi} \frac{e^{-m_{\rho(\pi)} |\mathbf{r}_1 - \mathbf{r}_2|}}{|\mathbf{r}_1 - \mathbf{r}_2|}, \quad (29)$$

and

$$\Sigma = \begin{pmatrix} \boldsymbol{\sigma} & 0 \\ 0 & \boldsymbol{\sigma} \end{pmatrix}. \quad (30)$$

For the ρ -meson density-dependent coupling strength we choose the functional form used in the DD-ME2 effective interaction [50]:

$$g_\rho(\rho_v) = g_\rho(\rho_{sat}) e^{-a_\rho(x-1)}, \quad (31)$$

with $x = \rho_v/\rho_{sat}$, and ρ_{sat} is the nucleon density at saturation in symmetric nuclear matter.

For the pseudovector pion-nucleon coupling we use the standard values: $f_\pi^2/4\pi = 0.08$, and $m_\pi = 138$ MeV. The derivative type of the pion-nucleon coupling necessitates the inclusion of the zero-range Landau-Migdal term, which accounts for the contact part of the nucleon-nucleon interaction

$$V_{\delta\pi} = g' \left(\frac{f_\pi}{m_\pi} \right)^2 \vec{\tau}_1 \vec{\tau}_2 \Sigma_1 \cdot \Sigma_2 \delta(\mathbf{r}_1 - \mathbf{r}_2), \quad (32)$$

with the parameter g' adjusted in such a way that the PN-RQRPA reproduces the experimental values of GTR excitation energies [44]. For the DD-ME2 effective interaction the value of $g'=0.52$ has been adjusted to the position of the GTR in ^{208}Pb .

In most applications of the RHB and RQRPA models [41, 42], the pairing part of the Gogny force has been used in the the pp -channel:

$$V^{pp}(1, 2) = \sum_{i=1,2} e^{-[(\mathbf{r}_1 - \mathbf{r}_2)/\mu_i]^2} (W_i + B_i P^\sigma - H_i P^\tau - M_i P^\sigma P^\tau), \quad (33)$$

with the set D1S [45] for the parameters μ_i , W_i , B_i , H_i and M_i ($i = 1, 2$). This force has been very carefully adjusted to pairing properties of finite nuclei all over the periodic table. In particular, the basic advantage of the Gogny force is the finite range, which automatically guarantees a proper cut-off in momentum space.

IV. ILLUSTRATIVE CALCULATIONS: CROSS SECTIONS FOR NEUTRINO DETECTOR RESPONSE

The theoretical framework described in the previous two sections can systematically be applied in studies of charged-current neutrino reaction rates with target nuclei of arbitrary mass. We have performed several illustrative calculations of cross sections for reactions with nuclei of interest for neutrino detector response: ^{12}C , ^{16}O , ^{56}Fe , and ^{208}Pb . The inclusive cross sections, which sum the contributions from transitions to all possible final states, are given as functions of neutrino energy, and can be averaged over the experimental neutrino flux when available, e.g. from the decay at rest of μ^+ , and the decay in flight of π^+ [6, 7, 8, 9, 10, 11]. The flux-averaged cross sections provide a crucial test for the validity of the theoretical approach used for modeling neutrino-nucleus reactions.

For charged-current reactions the cross section Eq. (2) must be corrected for the distortion of the outgoing lepton wave function by the Coulomb field of the daughter nucleus. In order to be able to compare our results with previous studies [22, 30], we use the same prescription for the Coulomb correction. The cross section can either be multiplied by a Fermi function obtained from the numerical solution of the Dirac equation for an extended nuclear charge distribution [30] or, at higher energies, the effect of the Coulomb field can be described by the effective momentum approximation (EMA) [51, 52, 53], in which the lepton momentum p_l and energy E_l are modified by a constant electrostatic potential evaluated at the center of the nucleus:

$$p_l^{eff} = \sqrt{E_l^{eff} - m_l^2} \quad (34)$$

$$E_l^{eff} = E_l - V_C(0), \quad (35)$$

where $V_C(0) = -3Z\alpha/(2r_c)$, the nuclear charge radius is denoted by r_c , and m_l is the mass of the outgoing lepton. In calculations with EMA the original lepton momentum p_l and energy E_l appearing in the expression for the cross section, are replaced by the above effective quantities.

The two prescriptions for the Coulomb correction are tested in the calculation of the inclusive cross section for neutrino scattering on a high-Z nucleus: $^{208}\text{Pb}(\nu_e, e^-)^{208}\text{Bi}$. In Fig. 1 we display the corresponding cross sections corrected either with the Fermi function, or calculated with the EMA. As already shown in previous studies, the Fermi function correction overestimates the cross sections at higher neutrino energies, where the EMA provides a more reliable correction. Therefore, following the prescription from Ref. [22], we will use the Fermi function correction in the range of neutrino energies for which the cross section is below the corresponding EMA value, whereas the EMA will be employed at higher energies (cf. the solid curve in Fig. 1).

One of the most extensively studied neutrino-nucleus reactions is $^{12}\text{C}(\nu_e, e^-)^{12}\text{N}$. This reaction is particularly important because ^{12}C is used in liquid scintillator detectors, and data on the cross section are available from the LSND [5, 6], and KARMEN [7, 8, 9] collaborations, as well as from LAMPF [10, 11]. In order to illustrate the contributions of different multipole excitations, in Fig. 2 we plot the inclusive cross section for the $^{12}\text{C}(\nu_e, e^-)^{12}\text{N}$ reaction as function of the neutrino energy, obtained by successively increasing the maximal allowed angular momentum in the sum over J in Eq. (5): from $J_{max} = 0^\pm$ to $J_{max} = 7^\pm$. One notices that the largest contributions arise from $J = 1^\pm$ and $J = 2^\pm$, and that the contribution of higher multipolarities gradually decreases. In fact, in this figure one can not distinguish the cross sections calculated with $J_{max} = 6^\pm$ and $J_{max} = 7^\pm$, for the whole interval of neutrino energies.

The results of model calculations can be compared with available data by averaging the cross section over the neutrino flux $f(E_\nu)$, which depends on the specific neutrino source

$$\langle \sigma_\nu \rangle = \frac{\int dE_\nu \sigma_\nu(E_\nu) f(E_\nu)}{\int dE'_\nu f(E'_\nu)}. \quad (36)$$

For ν_e the Michel flux from the decay at rest (DAR) of μ^+ is used [10],

$$f(E_{\nu_e}) = \frac{96 E_{\nu_e}^2}{m_\mu^4} (m_\mu - 2E_{\nu_e}), \quad (37)$$

whereas for ν_μ we employ the polynomial fit to the experimental flux obtained from the decay in flight (DIF) of π^+ [54]. In Table I the values of the muon and electron neutrino-nucleus cross sections for the reactions $^{12}\text{C}(\nu_e, e^-)^{12}\text{N}$ and $^{12}\text{C}(\nu_\mu, \mu^-)^{12}\text{N}$, calculated with the PN-RQRPA and averaged over the empirical neutrino fluxes, are compared with the results of previous theoretical studies based on the non-relativistic random phase approximation

and the shell model, and with the experimental values: LAMPF [10], KARMEN [8] and LSND [6, 54, 55]. For the (ν_μ, μ^-) reaction the PN-RQRPA cross section is in excellent agreement with the (Q)RPA results of Ref. [22], and the CRPA value of Ref. [29], but somewhat larger than the experimental cross section. The PN-RQRPA cross section for the $^{12}\text{C}(\nu_e, e^-)^{12}\text{N}$ reaction is in better agreement with experiment when compared with the results of the QRPA calculations [22, 38]. We notice that a very good agreement with data has been obtained in the shell-model calculations of Refs. [19, 22, 56], and with the RPA based on the Skyrme interactions SGII and SIII [20].

In Fig. 3 the calculated inclusive cross sections are plotted up to 100 MeV neutrino energy for three reactions including also heavier nuclei: $^{16}\text{O}(\nu_e, e^-)^{16}\text{F}$, $^{56}\text{Fe}(\nu_e, e^-)^{56}\text{Co}$, and $^{208}\text{Pb}(\nu_e, e^-)^{208}\text{Bi}$. The results of the RHB plus PN-RQRPA calculations are compared with those of a very recent analysis performed with the nonrelativistic QRPA and using the Skyrme interaction SIII [57]. First we notice the pronounced enhancement of cross sections for neutrino reactions on heavier nuclei: from ^{16}O to ^{208}Pb the reaction cross sections increase by more than two orders of magnitude. For the reaction on ^{16}O the present results are in excellent agreement with the QRPA - SIII cross sections [57] at all neutrino energies. This is also the case for the reactions on ^{56}Fe and ^{208}Pb at neutrino energies above 40 MeV, whereas at lower energies the RHB plus RQRPA cross sections appear somewhat below the QRPA results.

In table II we compare various theoretical results of flux-averaged cross sections for the electron neutrino reactions with ^{16}O , ^{56}Fe , and ^{208}Pb target nuclei. For the neutrino flux the DAR spectrum Eq. (37) is used, and values obtained with the shell model [56], the tensor model [59], Tamm-Dancoff [60], and various RPA-based calculations are included. For the ^{16}O target, the present PN-RQRPA(DD-ME2) cross section agrees with the shell model and (Q)RPA results. For heavier targets the differences between various calculations are more pronounced. Particularly important is the reaction $^{56}\text{Fe}(\nu_e, e^-)^{56}\text{Co}$, because it is the only case in which data are available for a medium-heavy target nucleus [9, 61]. The two self-consistent calculations: the QRPA [57] and the present RHB plus PN-RQRPA, which do not require any additional adjustments of the model parameters to the specific target nucleus, predict values for the cross section: $352 \times 10^{-42} \text{cm}^2$ (QRPA [57]) and $140 \times 10^{-42} \text{cm}^2$ (PN-RQRPA) which differ considerably, but are still within the uncertainties of the experimental result $(256 \pm 108 \pm 43) \times 10^{-42} \text{cm}^2$.

Obviously various theoretical approaches differ significantly in the predicted neutrino-nucleus cross sections, and this will require more detailed studies of the underlying nuclear structure that contributes to the neutrino reaction rates. On the other hand, the only data for a medium-heavy target nucleus are from the KARMEN collaboration [9], and this result has not yet been confirmed by independent measurement. One hopes that future experiments will provide additional constraints for theoretical models that are used in the description of weak interaction rates. At the same time the nuclear structure input for neutrino-nucleus cross sections must be further analyzed, and checked by improving the description of nuclear ground-state properties and spin-isospin excitations relevant for the calculation of the reaction rates.

Next we consider in more detail the contributions from excitations of various multiplicities to the neutrino-nucleus cross sections evaluated within the RHB plus PN-RQRPA framework. Fig. 4 displays the calculated cross sections for the reaction $^{56}\text{Fe}(\nu_e, e^-)^{56}\text{Co}$. The solid curve represents the inclusive cross section as a function of the neutrino energy calculated by including all multipole transitions with $J \leq 7^\pm$, whereas the dashed curve corresponds to the cross section evaluated only for transitions to the isobaric analog state (IAS) and Gamow-Teller (GT) resonance. The difference between these two cases is represented by the dotted curve which, as one notes, rises sharply with energy. Below an incident neutrino energy of $E_{\nu_e} \approx 30$ MeV the dominant contribution to the cross section originates from the two basic charge exchange modes: IAS and GTR. With increasing E_{ν_e} , however, contributions from other multipole transitions become even more important. This result clearly shows that models which take into account only the IAS and GTR transitions [62], cannot provide quantitative predictions of cross sections at neutrino energies $E_{\nu_e} \geq 30$ MeV.

The contribution of different multipole transitions to the cross section for the reaction $^{56}\text{Fe}(\nu_e, e^-)^{56}\text{Co}$, at increasing neutrino energies, is illustrated in Fig. 5. For the neutrino energies $E_{\nu_e} = 20, 40, 60,$ and 80 MeV, we display the partial contributions to the total cross section of multipoles from $J = 0^\pm$ to $J = 5^\pm$. At $E_{\nu_e} = 20$ MeV the reaction is dominated by transitions to the IAS and GTR. At higher energies, however, other multiplicities start to play an important role and one notices, in particular, the dominant contribution of the 1^- transitions at $E_{\nu_e} = 60$ and 80 MeV. This distribution of multipole transitions, calculated in the RHB plus PN-RQRPA model, is similar to the one obtained in the QRPA with Skyrme effective interactions [57]. The differences in the contributions of higher multipoles can be

attributed to the different effective interactions employed in the two models.

V. CROSS SECTIONS FOR SUPERNOVA NEUTRINOS

An important application of microscopic models of neutrino-nucleus reactions is the calculation of cross sections for supernova neutrinos. Accurate modeling of reaction rates on nuclei that can be used as targets for the supernova neutrino detectors is, of course, essential for studies of supernova dynamics and, in particular, of weak interaction processes which determine the evolution of a supernova explosion. In this section we compare the results of illustrative RHB plus PN-RQRPA calculations of charged-current reaction rates with those obtained in the shell model [17], and with the CRPA [30]. The supernova neutrino flux is usually described by the Fermi-Dirac spectrum:

$$f(E_\nu) = \frac{1}{T^3} \frac{E_\nu^2}{\exp[(E_\nu/T) - \alpha] + 1}. \quad (38)$$

At typical supernova neutrino energies one expects the total cross section for the charged current reaction (ν_e, e^-) to be dominated by the allowed transitions to the IAS and the Gamow-Teller resonance states in the daughter nucleus. In Fig. 6 we display the flux-averaged cross sections for the reaction $^{16}\text{O}(\nu_e, e^-)^{16}\text{F}$, evaluated at different temperatures in the interval $T = 2 - 10$ MeV, and for the chemical potential $\alpha=0$. The results are in a remarkable agreement with those obtained in the shell-model calculation of Ref. [17]. This is a very interesting result, because the two models are based on entirely different concepts, and use different effective interactions. An important advantage of the present approach, however, is that it can easily be extended to heavier nuclei and to systems far from stability, and therefore also applied in the description of the r -process nucleosynthesis.

We have further tested the model in the case of the heavy target: $^{208}\text{Pb}(\nu_e, e^-)^{208}\text{Bi}$. For the same neutrino flux as in the previous example, the corresponding cross sections are shown in Fig. 7 and compared, at $T = 6, 8$ and 10 MeV, with the results from Refs. [22, 30, 63]. Since at higher temperatures the neutrino flux extends toward higher neutrino energies, the calculated cross sections display a pronounced enhancement with temperature (cf. Sec. IV). In comparison with the RPA-based results from Refs. [22, 30], the present PN-RQRPA calculation predicts a slightly lower value for the flux-averaged cross section at $T = 6$ MeV, whereas an excellent agreement is obtained at $T = 8$ and 10 MeV. Note that the calculation

of Ref. [63], which includes the IAS, the GT, and the first-forbidden transitions computed in the Goldhaber-Teller model, consistently predicts higher values for the flux-averaged cross section at all considered temperatures. As it has already been discussed in Ref. [23], a possible origin of this difference could be the use of the Fermi function for the Coulomb correction at higher neutrino energies, instead of the EMA.

Although most calculations of neutrino-nucleus cross sections consider only the case when the chemical potential $\alpha=0$, in astrophysical applications it might be important to perform studies of reaction rates for other values of α [30]. We have therefore explored the sensitivity of the neutrino reaction cross sections to α . In Fig. 8 the contour plot is shown for the $^{16}\text{O}(\nu_e, e^-)^{16}\text{F}$ cross sections as functions of T and α in the Fermi-Dirac spectrum of Eq. (38). The curves in the plot correspond to constant values of the cross sections. At lower temperatures the cross sections depend only very weakly on α . However, already above $T=2$ MeV, the cross sections increase much faster for higher values of the chemical potential α .

VI. CONCLUDING REMARKS

Detailed microscopic calculations of charged-current and neutral-current neutrino-nucleus reaction rates are of crucial importance for models of neutrino oscillations, detection of supernova neutrinos, and studies of the r-process nucleosynthesis. In this work we have introduced a consistent microscopic method for calculating neutrino-nucleus cross sections, based on the relativistic mean-field framework. In this approach the ground state of a nucleus is described with the relativistic Hartree-Bogoliubov model, and the neutrino-induced transitions to excited nuclear states are computed in the relativistic quasiparticle random phase approximation. Since it is based on the self-consistent mean-field approach to nuclear structure, the model can be applied to neutrino reactions with target nuclei of arbitrary mass throughout the chart of nuclides. By employing universal effective interactions, with parameters adjusted to global nuclear properties, the calculation of neutrino-nucleus cross sections is essentially parameter free. In the particular model introduced in this work, once the ground state of a target nucleus is calculated with the RHB model, the only additional parameter in the PN-QRPA calculations of excited states is the strength g' of the zero-range Landau-Migdal term, which accounts for the contact part of the nucleon-nucleon interaction. The value of this parameter depends on the isovector properties (symmetry energy) of the

effective interaction in the particle-hole channel, and is adjusted to reproduce the excitation energy of the GTR in ^{208}Pb . The same value of g' is then used in calculations of charge-exchange excitations in all other nuclei. Since it does not contain parameters adjusted to specific target nuclei, or even to a particular mass region, the model can be extended to regions of nuclei far from stability for which no data on ground and/or excited states are available, including those on the path of the r-process.

We have performed a number of illustrative test calculations for charged-current neutrino reactions on ^{12}C , ^{16}O , ^{56}Fe , and ^{208}Pb , in the low-energy range below 100 MeV neutrino energy. The results have been compared with those obtained in previous theoretical studies based on the shell model and the non-relativistic random phase approximation, and with the available experimental values for flux-averaged cross sections. In addition to the total neutrino-nucleus cross sections, we have also analyzed the evolution of the contributions of different multipole excitations as a function of neutrino energy. It has been shown that except at relatively low neutrino energies $E \leq 30$ MeV, for which the reactions are dominated by transitions to IAS and GTR states, at higher energies the inclusion of spin-dipole transitions, and also excitations of higher multiplicities, is essential for a quantitative description of neutrino-nucleus cross sections. Finally, we have also investigated the cross sections for reactions of supernova neutrinos on ^{16}O and ^{208}Pb target nuclei as functions of the temperature and chemical potential.

The results for the test cases are in good agreement with the few available data, and with the cross sections calculated in the shell model for reactions on light nuclei. The advantage of the RHB plus PN-RQRPA model over the shell model approach is, of course, the possibility of performing calculations for reactions on heavier nuclei and in regions of nuclei far from stability. The differences between the results of various RPA-based calculations, especially in heavier nuclei and at low neutrino energies, can most probably be attributed to the different effective interactions used in modeling the structure of target nuclei, but they also indicate that more detailed experimental and theoretical studies of the transitions that contribute to the neutrino reaction rates must be performed.

After the present test study, future applications of the RHB plus PN-RQRPA model will include a more extensive investigation of charged-current neutrino-nucleus reaction rates, as well as processes induced by neutral-current neutrino reactions, and neutrino nucleosynthesis.

ACKNOWLEDGMENTS

This work has been supported in part by MZOS - project 1191005-1010, and by the DFG Cluster of Excellence “Origin and Structure of the Universe”.

- [1] A. C. Hayes, *Phys. Rep.* 315, 257 (1999).
- [2] S. Freedman, B. Kayser et al., ”The Neutrino Matrix: DNP/DPF/DAP/DPB Joint Study on the Future of Neutrino Physics”, Technical Report, American Physical Society (2004).
- [3] A. Heger, E. Kolbe, W. C. Haxton, K. Langanke, G. Martínez Pinedo, and S. E. Woosely, *Phys. Lett. B* 606, 258 (2005).
- [4] K. Langanke, *Prog. Part. Nucl. Phys.* 57, 324 (2006).
- [5] M. Albert et al., *Phys. Rev. C* 51, R1065 (1995).
- [6] C. Athanassopoulos et al., *Phys. Rev. C* 55, 2078 (1997).
- [7] B. E. Bodmann et al., *Phys. Lett. B* 280, 198 (1992).
- [8] B. E. Bodmann et al., *Phys. Lett. B* 332, 251 (1994).
- [9] R. Maschuw, *Prog. Part. Nucl. Phys.* 40, 183 (1998).
- [10] D. A. Krakauer et al., *Phys. Rev. C* 45, 2450 (1992).
- [11] D. D. Koetke et al., *Phys. Rev. C* 46, 2554 (1992).
- [12] F. T. Avignone, L. Chatterjee, Yu. V. Efremenko, M. Strayer, *J. Phys. G* 29, 2497 (2003).
- [13] Yu. V. Efremenko, *Nucl. Phys. B* 138, 343 (2005).
- [14] P. Zucchelli, *Phys. Lett. B* 532, 166 (2002).
- [15] C. Volpe, *J. Phys. G* 30, L1 (2004).
- [16] G. C. McLaughlin, *Phys. Rev. C* 70, 045804 (2004).
- [17] W. C. Haxton, *Phys. Rev. D* 36, 2283 (1987).
- [18] J. Engel, E. Kolbe, K. Langanke, and P. Vogel, *Phys. Rev. C* 54, 2740 (1996).
- [19] A. C. Hayes and I. S. Towner, *Phys. Rev. C* 61, 044603 (2000).
- [20] N. Auerbach, N. Van Giai, and O. K. Vorov, *Phys. Rev. C* 56, R2368 (1997).
- [21] S. K. Singh, N. C. Mukhopadhyay, and E. Oset, *Phys. Rev. C* 57, 2687 (1998).
- [22] C. Volpe, N. Auerbach, G. Colò, T. Suzuki, and N. Van Giai, *Phys. Rev. C* 62, 015501 (2000).
- [23] C. Volpe, N. Auerbach, G. Colò, and N. Van Giai, *Phys. Rev. C* 65, 044603 (2002).
- [24] E. Kolbe, K. Langanke, S. Krewald, F.-K. Thielemann, *Nucl. Phys. A* 540, 599 (1992).

- [25] E. Kolbe, K. Langanke, F.-K. Thielemann, and P. Vogel, *Phys. Rev. C* 52, 3437 (1995).
- [26] N. Jachowicz, S. Rombouts, K. Heyde, and J. Ryckebusch, *Phys. Rev. C* 59, 3246 (1999).
- [27] N. Jachowicz, K. Heyde, J. Ryckebusch, and S. Rombouts, *Phys. Rev. C* 65, 025501 (2002).
- [28] A. Botrugno and G. Co', *Nucl. Phys. A* 761, 200 (2005).
- [29] E. Kolbe, K. Langanke, and P. Vogel, *Nucl. Phys. A* 652, 91 (1999).
- [30] E. Kolbe, K. Langanke, G. Martínez-Pinedo, and P. Vogel, *J. Phys. G* 29, 2569 (2003).
- [31] J. D. Walecka *Muon Physics*, edited by V. M. Hughes and C. S. Wu, Academic, New York (1975).
- [32] T. K. Gaisser and J. S. O'Connell, *Phys. Rev. D* 34, 822 (1986).
- [33] T. Kuramoto, M. Fukugita, Y. Kohyama, and K. Kubodera, *Nucl. Phys. A* 512, 711 (1990).
- [34] S. Fracasso and G. Colò, *Phys. Rev.* 72, 064310 (2005).
- [35] A. C. Hayes, P. Navrátil, and J. P. Vary, *Phys. Rev. Lett.* 91, 012502 (2003).
- [36] T. Suzuki, S. Chiba, T. Yoshida, T. Kajino, and T. Otsuka, *Phys. Rev. C* 74, 034307 (2006).
- [37] A. Samana, F. Krmpotić, A. Mariano, R. Zukanovich Funchal, *Phys. Lett. B* 642, 100 (2006).
- [38] F. Krmpotić, A. Samana, and A. Mariano, *Phys. Rev. C* 71, 044319 (2005).
- [39] J. S. O'Connell, T. W. Donnelly, and J. D. Walecka, *Phys. Rev. C* 6, 719 (1972).
- [40] T. W. Donnelly and W. C. Haxton, *At. Data Nucl. Data Tables* 25, 1 (1980).
- [41] D. Vretenar, A. V. Afanasjev, G. A. Lalazissis, and P. Ring, *Phys. Rep.* 409, 101 (2005).
- [42] N. Paar, D. Vretenar, E. Khan, and G. Colò, *Rep. Prog. Phys.* 70, 691 (2007).
- [43] N. Paar, P. Ring, T. Nikšić, and D. Vretenar, *Phys. Rev. C* 67, 034312 (2003).
- [44] N. Paar, T. Nikšić, D. Vretenar, and P. Ring, *Phys. Rev. C* 69, 054303 (2004).
- [45] J. F. Berger, M. Girod, and D. Gogny, *Comp. Phys. Comm.* 63, 365 (1991).
- [46] D. Vretenar, N. Paar, T. Nikšić, and P. Ring, *Phys. Rev. Lett.* 91, 262502 (2003).
- [47] T. Nikšić, T. Marketin, D. Vretenar, N. Paar, and P. Ring, *Phys. Rev. C* 71, 014308 (2005).
- [48] T. Marketin, D. Vretenar, and P. Ring, *Phys. Rev. C* 75, 024304 (2007).
- [49] J. Engel, M. Bender, J. Dobaczewski, W. Nazarewicz, and R. Surman, *Phys. Rev. C* 60, 014302 (1999).
- [50] G. A. Lalazissis, T. Nikšić, D. Vretenar, and P. Ring, *Phys. Rev. C* 71, 024312 (2005).
- [51] J. Engel, *Phys. Rev. C* 57, 2004 (1998).
- [52] M. Traini, *Nucl. Phys. A* 694, 325 (2001).
- [53] A. Aste and J. Jourdan, *Europhys. Lett.* 67, 753 (2004).

- [54] C. Athanassopoulos et al., Phys. Rev. Lett. 81, 1774 (1998).
- [55] L.-B. Auerbach et al., Phys. Rev. C 64, 065501 (2001).
- [56] N. Auerbach and B. A. Brown, Phys. Rev. C 65, 024322 (2002).
- [57] R. Lazauskas and C. Volpe *arXiv:0704.2724v1 [nucl-th]* (2007).
- [58] M. S. Athar, S. Ahmad, and S. K. Singh, Nucl. Phys. A 764, 551 (2006).
- [59] S. L. Mintz, J. Phys. G 28, 451 (2002).
- [60] T. Suzuki, H. Sagawa, Nucl. Phys. A 718, 446c (2003).
- [61] E. Kolbe and K. Langanke, Phys. Rev. C 63, 025802 (2001).
- [62] I. N. Borzov and S. Goriely, Phys. Rev. C 62, 035501 (2000).
- [63] G. M. Fuller, W. C. Haxton, and G. C. McLaughlin, Phys. Rev. D 59, 085005 (1999).

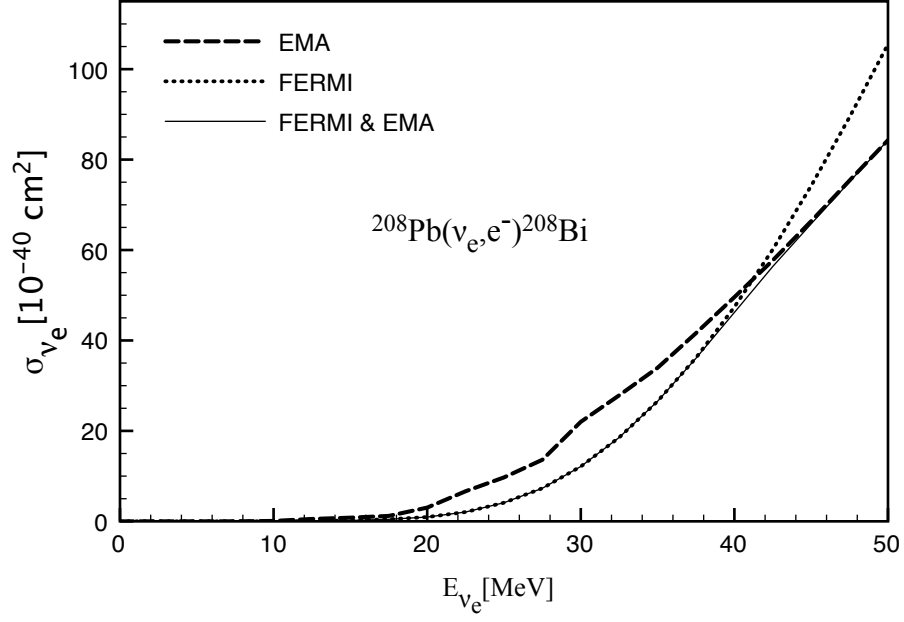


FIG. 1: Inclusive neutrino-nucleus cross sections for the $^{208}\text{Pb}(\nu_e, e^-)^{208}\text{Bi}$ reaction, evaluated using the effective momentum approximation (dashed), the Fermi function correction (dotted), and their combination (solid). The PN-RQRPA calculation is performed with the DD-ME2 effective interaction.

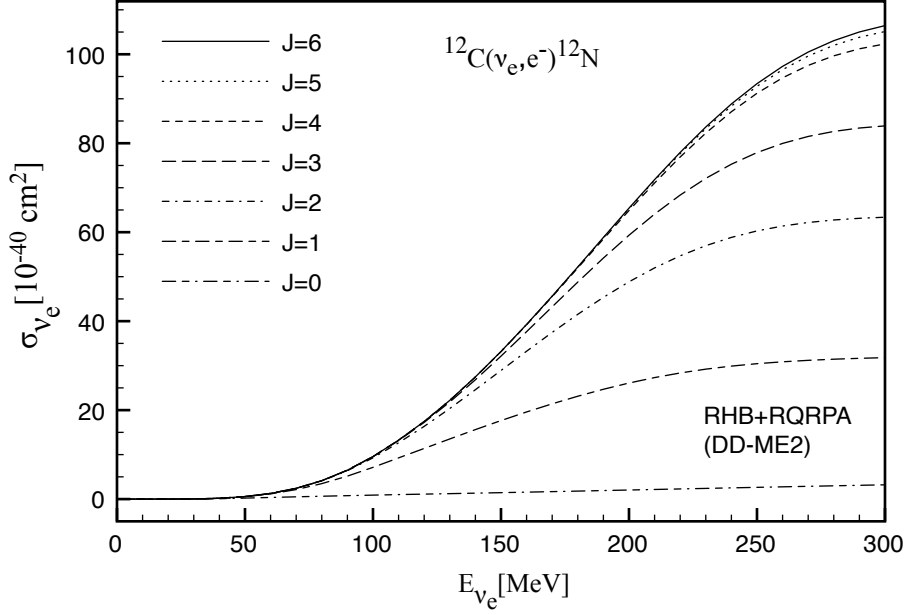


FIG. 2: The RHB plus PN-RQRPA inclusive neutrino-nucleus cross sections for the $^{12}\text{C}(\nu_e, e^-)^{12}\text{N}$ reaction. The different curves correspond to cross sections evaluated by successively increasing the maximal allowed angular momentum in the sum over J in Eq. (5): from $J_{max} = 0^\pm$ to $J_{max} = 7^\pm$.

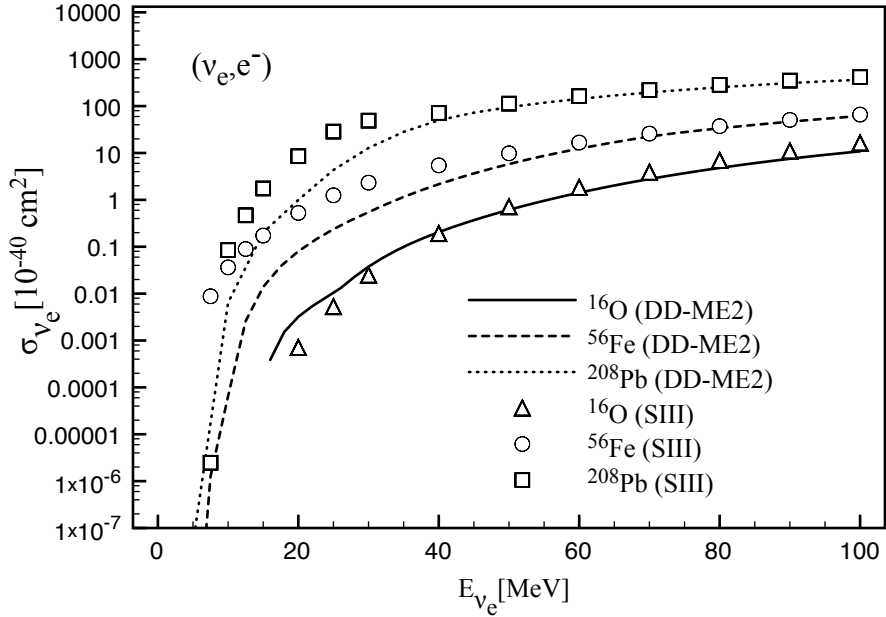


FIG. 3: Inclusive cross sections for the $^{16}\text{O}(\nu_e, e^-)^{16}\text{F}$, $^{40}\text{Ar}(\nu_e, e^-)^{40}\text{K}$, and $^{208}\text{Pb}(\nu_e, e^-)^{208}\text{Bi}$ reactions. The RHB plus PN-RQRPA(DD-ME2) results are compared with those obtained in the QRPA with the Skyrme interaction SIII [57].

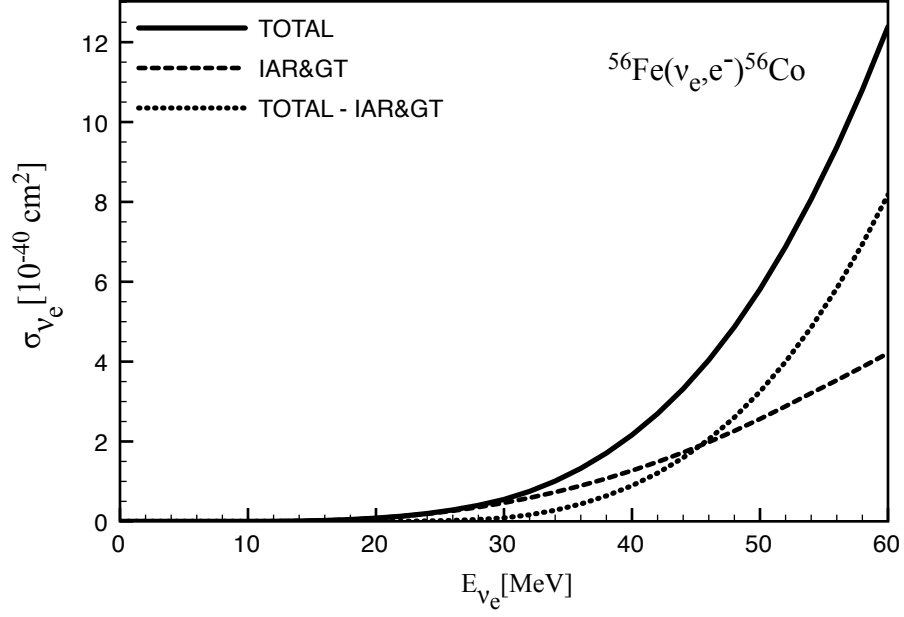


FIG. 4: Inclusive cross section for the $^{56}\text{Fe}(\nu_e, e^-)^{56}\text{Co}$ reaction. The solid curve corresponds to the full calculation including all transitions with multipolarity $J \leq 7^\pm$, whereas the cross section evaluated for the IAS and GT transitions only is represented by the dashed curve. The dotted curve is the difference between the two calculations.

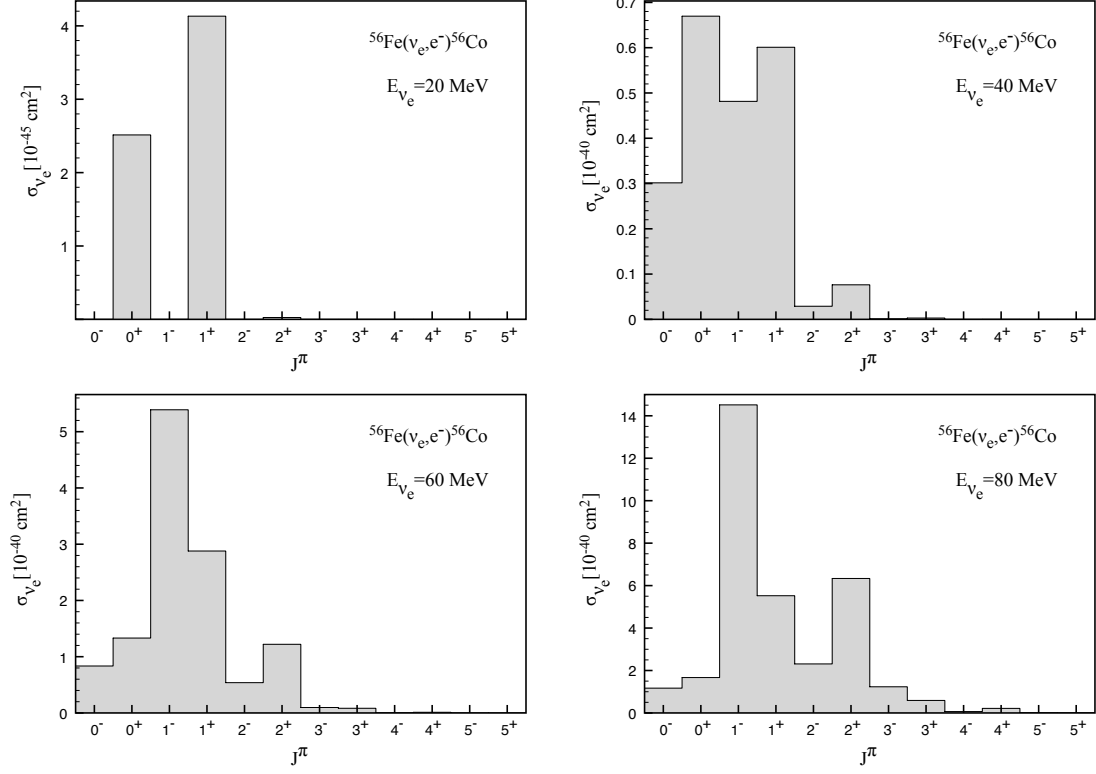


FIG. 5: Contributions of different multipole transitions to the RHB plus PN-RQRPA inclusive cross section for the $^{56}\text{Fe}(\nu_e, e^-)^{56}\text{Co}$ reaction, at the incoming electron neutrino energies $E_{\nu_e} = 20, 40, 60,$ and 80 MeV .

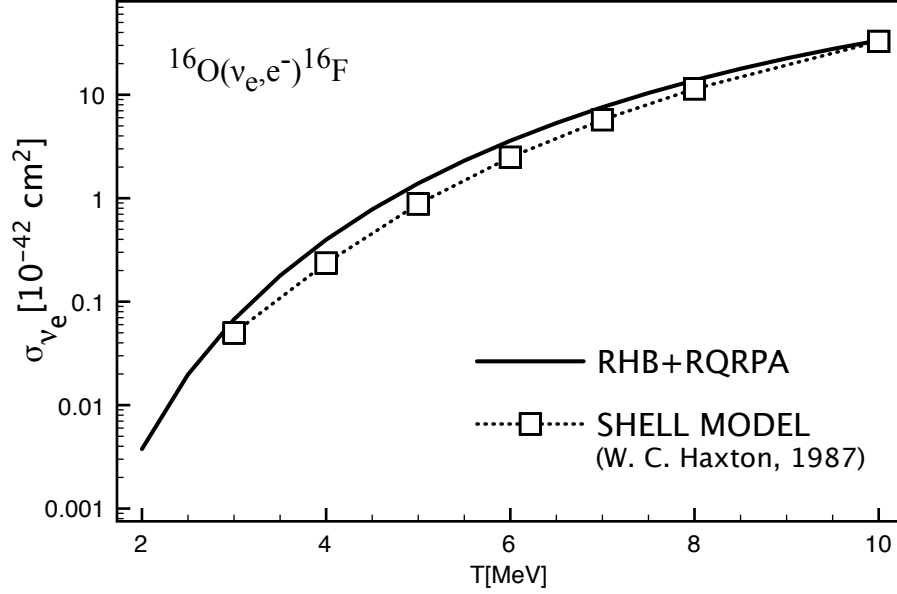


FIG. 6: Inclusive cross section for the $^{16}\text{O}(\nu_e, e^-)^{16}\text{F}$ reaction, averaged over the supernova neutrino flux and plotted as a function of temperature. The PN-RRPA results obtained with the DD-ME2 effective interaction are compared with the shell-model cross-sections from Ref. [17].

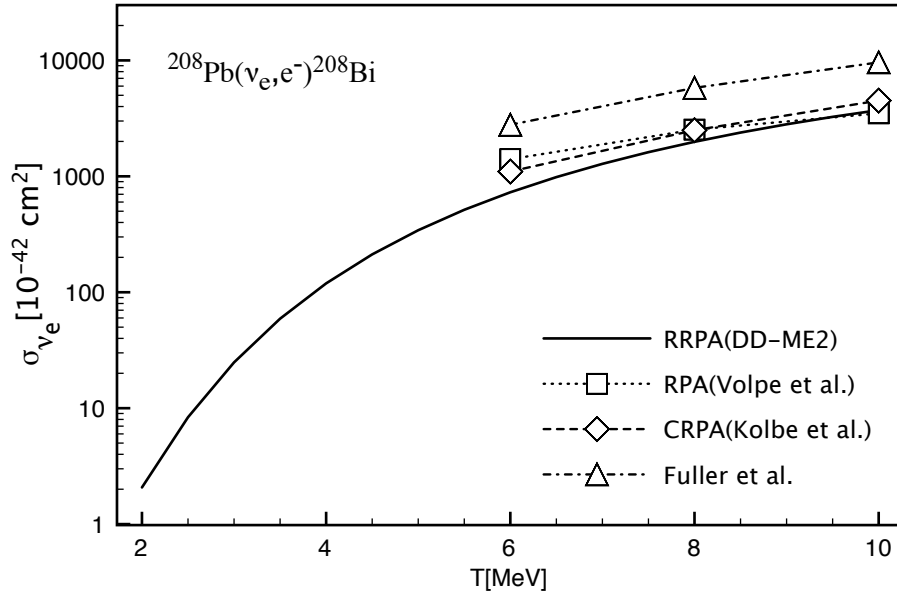


FIG. 7: Same as in Fig. 6, but for the $^{208}\text{Pb}(\nu_e, e^-)^{208}\text{Bi}$ reaction, in comparison with the results from Refs. [22, 30, 63].

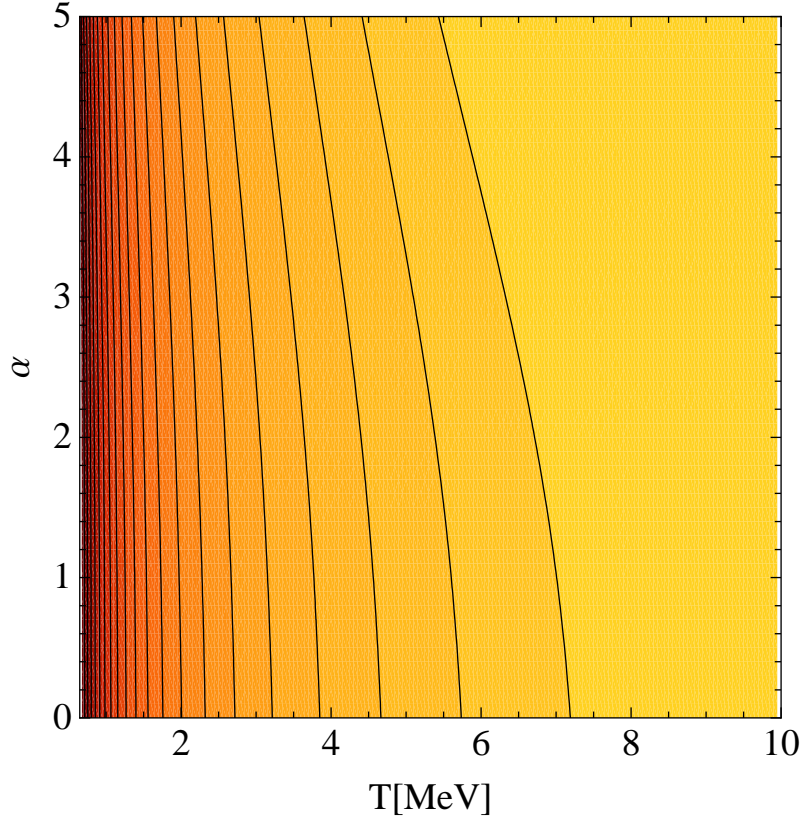


FIG. 8: Contour plot of supernova neutrino-nucleus cross sections for the $^{16}\text{O}(\nu_e, e^-)^{16}\text{F}$ reaction, as functions of the temperature T and chemical potential α which determine the Fermi-Dirac neutrino spectrum Eq. (38). The solid curves in the plot correspond to constant values of the cross section, and lighter shading denotes the increase of cross sections.

TABLE I: Flux-averaged neutrino-nucleus cross sections for the ^{12}C target nucleus. The results of several shell-model and QRPA based calculations, including the present PN-RQRPA(DD-ME2), are compared with available data.

	(ν_μ, μ^-)	(ν_e, e^-)
	$\langle\sigma\rangle(10^{-40}\text{cm}^2)$	$\langle\sigma\rangle(10^{-42}\text{cm}^2)$
RPA(SIII) [22]	19.23	55.10
QRPA(SIII) [22]	20.29	52.0
CRPA(WS+LM) [29]	18.18	19.28
PQRPA(PIII) [38]		17.54
RPA [58]		13.60
RPA(SGII) [20]	13.5	12.9
RPA(SIII) [20]	14.5	16.5
SM(WS(0+1+2+3) $\hbar\omega$) [19]	13.2	12.3
SM(0 $\hbar\omega \times 0.64$) [56]	19.2	15.1
SM(HF(0+1+2+3) $\hbar\omega$) [22]	15.18	16.42
PN-RQRPA(DD-ME2)	19.59	12.14
Exp.(KARMEN) [8]		14.0 \pm 1.2
Exp.(LSND) [54, 55]	12.4 \pm 0.3 \pm 1.8	13.2 \pm 0.4 \pm 0.6
Exp.(LAMPF) [10]		14.1 \pm 2.3

TABLE II: Flux-averaged cross sections for the ν_e reaction on ^{16}O , ^{56}Fe , and ^{208}Pb target nuclei.

	$^{16}\text{O}(\nu_e, e^-)^{16}\text{F}$	$^{56}\text{Fe}(\nu_e, e^-)^{56}\text{Co}$	$^{208}\text{Pb}(\nu_e, e^-)^{208}\text{Bi}$
	$\langle\sigma\rangle(10^{-42}\text{cm}^2)$	$\langle\sigma\rangle(10^{-42}\text{cm}^2)$	$\langle\sigma\rangle(10^{-42}\text{cm}^2)$
SM($0\hbar\omega \times 0.64$) [56]	10.8		
TM [59]		214	
TDA(SKIII) [60]			2954,3204
RPA [58]	14.55	277	2643
CRPA(WS+LM) [61]		240	3620
(Q)RPA(SIII,SGII)	16.90,17.20 [20]	352 [57]	4439 [23]
PN-RQRPA(DD-ME2)	13.18	140	2812
Exp.(KARMEN) [9, 61]		$256\pm 108\pm 43$	